ACS APPLIED ENERGY MATERIALS

www.acsaem.org
Article

Electrochemical Performance of Engineered $NiCo_2O_4$ in AEM Water Electrolyzers: Direct-Growth vs Spray-Coated Anode

Ataollah Niyati, Arianna Moranda, Sebastiano Bellani, Thi Hong Hanh Le, Michele Ferri, and Ombretta Paladino*

Cite This: https://doi.org/10.1021/acsaem.5c01487
Read Online

ABSTRACT: This study investigates the synthesis and electrochemical performance of $NiCo_2O_4$ anodes for water electrolysis in both alkaline and anion exchange membrane (AEM) configurations. An engineered direct growth method using a urea-mediated sono-hydrothermal approach was used to synthesize $NiCo_2O_4$ on Ni felt, creating a binder-free electrode optimized for an alkaline environment. We evaluated the electrode's performance in AEM water electrolysis, comparing it with a spray-coated electrode incorporating ionomers and the same electrocatalyst. Our findings highlight that direct-grown binder-free electrodes, produced through varied synthesis routes, exhibit remarkable activity and stability in AEM cells operated in dry cathode mode (1.90 V @ 1 A cm^{-2}), with seamless interaction between the catalyst layer and the membrane. Moreover, this binder-free $NiCo_2O_4$ on Ni felt is also an efficient anode under alkaline electrolysis configuration, exhibiting high stability and remarkable performance (1.78 V @ 1 A cm^{-2}, 1.92 V @ 2 A cm^{-2}), ascribable to the increased conductivity and improved charge transfer resistance of the catalyst layer.

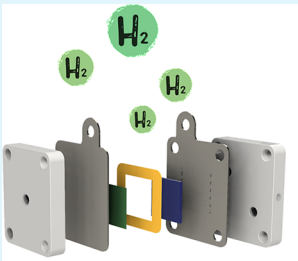

MEA of Electrolyzer for AEM and AEL

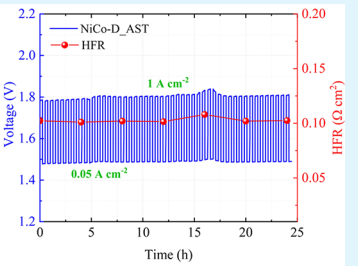

AEL 24-hr Accelerated Stress Test

KEYWORDS: *anion exchange membrane water electrolysis, alkaline water electrolysis, green hydrogen production, oxygen evolution reaction, $NiCo_2O_4$, sono-hydrothermal method, binder-free*

1. INTRODUCTION

In today's world, sustainable energy solutions have brought attention due to the importance of not only hydrogen production technologies but also alternative fuel synthesis.[1] To this end, water electrolysis stands out as a reliable approach for producing green hydrogen for achieving zero emissions by serving as a clean fuel or, most likely, as a chemical feedstock.[2,3] Among several electrolysis setups, alkaline water electrolysis seems to be an efficient and well-established technology due to its unique characteristics such as simplicity, low cost, and high stability under operation.[4,5] However, alkaline water electrolyzers (AELs) face several drawbacks when paired with intermittent renewable energy sources, such as wind and solar power. These include: (i) slow dynamic response, especially under atmospheric pressure, which can limit the efficiency and result in inconsistent hydrogen production[6]; (ii) need for implementing strategies to maintain a continuous operation or partial load, operation through complementary storage units, as frequent start−stop cycles caused by the variable output of renewables and associated with temporary reverse polarization can lead to mechanical stress and degradation of AEL components, particularly electrodes[7,8]; (iii) limited part-load efficiency since at lower loads, excessive gas crossover can occur, compromising safety and potentially leading to shutdowns, which further limits flexibility in fluctuating power conditions.[9−11]

On the one hand, anion exchange membrane water electrolyzers (AEM-WEs) and proton exchange membrane electrolyzers (PEM-WEs) are generally considered to be more resilient when operated with intermittent energy sources due to their quicker dynamic response, higher efficiency at part-load, and better adaptability to fluctuating power inputs, making them more compatible with renewable energy sources than conventional systems such as alkaline electrolyzer.[12−15] They have a higher power density and can also operate under differential pressure, making them ideal for reducing postproduction costs associated with hydrogen gas compression. In this context, AEM-WEs combine several advantages of both AELs and PEM-WEs, while offering additional benefits, such as compatibility with a broader range of catalysts and higher operating flexibility. In particular, AEM-WEs do not necessarily require the presence of precious metal catalysts

Received: May 17, 2025
Revised: July 3, 2025
Accepted: July 31, 2025

such as Pd and Pt, or allow the reduction of the load of these metals, significantly decreasing overall system costs while (ideally) eliminating the need for several critical raw materials.[16−18] Despite these benefits, the success of AEM-WE technology is still linked to the understanding of the electrode−membrane interface and the role of ionomers in facilitating efficient ion transfer.[19−21] The presence of ionomers in AEM-WE fed with pure water seems to be essential, as they are the only ionic conductors.[22] Conversely, when operating AEM-WEs with alkaline electrolytes (e.g., 1 M KOH), binder-free electrodes could show better performance, as the absence of ionomers avoids blockage of the catalyst active sites and the decrease of electronic conductivity of the catalyst layer. However, the overall impact of ionomers on cell stability and efficiency needs further investigation.[22]

In this study, we focus on the performance assessment of morphology-engineered $NiCo_2O_4$-based anodes produced as both freestanding, binder-free electrodes, obtained by direct growth onto the substrate, and their ionomer-containing counterparts, obtained by spray-coating. Both electrodes have been tested in zero-gap AEL and AEM-WE configurations. $NiCo_2O_4$ is recognized for its excellent electrochemical activity in oxygen evolution reactions (OER), due to its chemical stability and relatively low cost, making it a strong candidate for integration into commercial electrolysis systems.[23−26] To synthesize $NiCo_2O_4$, we use the sono-hydrothermal approach, a versatile technique that enables the production of highly crystalline nanostructures with controlled morphology and dispersion to achieve nanorods with particle size between 20 to 45 nm.[27,28] In particular, the sono-hydrothermal process allows for the direct growth of $NiCo_2O_4$ on Ni felt, creating a binder-free, high-surface-area electrode specifically designed for enhanced performance in AELs.[29]

However, given the promising attributes of AEM-WEs, we sought to extend the application of our engineered $NiCo_2O_4$-based anodes to AEM-WEs, where the presence of an ionomer in the electrodes and the engineering of catalyst-membrane interfaces typically play a central role in determining the overall cell performance. To this end, we prepared $NiCo_2O_4$-based electrodes through both direct growth and spray-coating techniques, with the latter involving the use of ionomers that may enhance the electrode/AEM interactions by establishing continuous anion-conducting pathways. Spray-coating is a widely adopted technique for the fabrication of AEM-WE electrodes, allowing for the precise control of catalyst layer thickness and distribution over the substrate surface.[30−33] In this work, $NiCo_2O_4$ powders synthesized through the sono-hydrothermal method were formulated into inks containing an ionomer and subsequently spray-coated onto the Ni felt substrates. Through comparative analysis of the two fabrication techniques, we aim to elucidate the influence of ionomer on the electrode performance and stability in both AEL and AEM-WE cells.

2. EXPERIMENTAL SECTION

2.1. Materials. $NiCl_2{\cdot}6H_2O$ (99% purity, Carlo Erba Reagents, Italy) and $CoCl_2{\cdot}6H_2O$ (98% purity, Carlo Erba Reagents, Italy) served as Ni and Co precursors. KOH (99% purity, Carlo Erba Reagents, Italy) and urea (99% purity, Carlo Erba Reagents, Italy) were used for the electrocatalyst synthesis as well as the electrolyte source. Additionally, 10 wt % Nafion dispersion (D1021 Nafion, Fuel Cell Store, USA) and Zirfon Perl UTP 220 diaphragm (Agfa) were adopted for AEL; while Aemion+ AF3-HWK9-75-X AEM and related ionomer (Ionomr Innovations, Canada) and Pt/C (30 wt %, from Cabro S.p.A., Italy) were used in AEM-WE cells. Ethanol (EtOH), 2-propanol (IPA) were purchased from Sigma-Aldrich (Germany). Ni felts (99% pure nickel, 1 mm thickness, porosity 0.85) gas diffusion layers supplied from QL Metal Fiber Co (China) were used to fabricate the electrodes.

2.2. Direct-Growth Preparation of Electrodes for the OER. The engineered catalyst and electrodes are produced by following the methodology described in Niyati et al.[34] The direct growth method is a binder-free method to coat directly the electrocatalyst ($NiCo_2O_4$) onto the surface of the Ni felt, as illustrated in Figure 1.

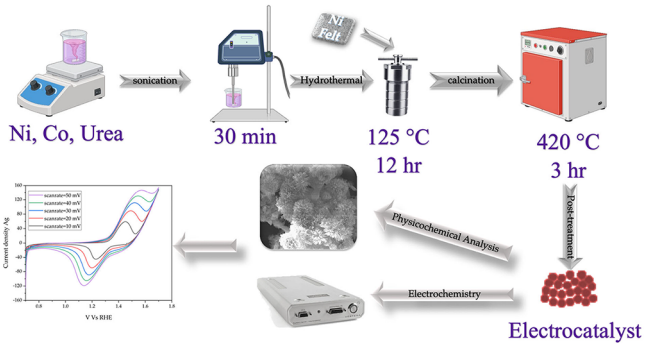

Figure 1. Synthesis of $NiCo_2O_4$ powder and fabrication of the NiCo-D electrode via a urea-mediated sono-hydrothermal process.

Experimentally, Ni felt was first immersed in a solution of 3 M HCl for 5 min, followed by rinsing in a mixture of Milli-Q water and acetone for 15 min with sonication. After cleaning, it was dried overnight in a vacuum oven at 60 °C. The dried Ni felt was weighed before and after the sonothermal process so as to accurately determine the amount of catalyst loaded on the electrode through the direct growth method.

The $NiCo_2O_4$ electrocatalyst was synthesized using a design of experiments (DOE) approach to optimize the operating conditions of the sono-hydrothermal process and using urea as a hydrolysis agent, as described in Paladino et al.[27] To synthesize the $NiCo_2O_4$ electrocatalyst, 2.015 g of $NiCl_2{\cdot}6H_2O$ was dissolved in 25 mL of Milli-Q water and slowly added dropwise to a $CoCl_2{\cdot}6H_2O$ solution containing 4.0354 g of Co precursor in 40 mL of Milli-Q water. In the second step, urea was added in a 1:10 molar ratio, and the solution was vigorously stirred for 30 min. To enhance nucleation and nanoparticle formation, the solution was subjected to sonication at 100 W for an additional 30 min. The resulting solution was then transferred to a 100 mL Teflon-lined stainless-steel autoclave for the hydrothermal reaction. Clean Ni felt was placed inside the autoclave, and the reaction was carried out at 125 °C for 12 h. After the completion of the reaction, the electrode was thoroughly washed with Milli-Q water and ethanol to remove any residual impurities or excess $NiCo_2O_4$. The powder of $NiCo_2O_4$ was collected by filtration and washed with ethanol and Milli-Q water to be used for spray coating. Both the collected powder and electrode were then dried overnight in a vacuum oven at 60 °C. In the final step, the dried powder and Ni felt underwent thermal treatment in air at 420 °C for 3 h with a heating ramp of 10 °C/min. This process ensured the successful synthesis of $NiCo_2O_4$ with the desired characteristics for subsequent analysis and application. Through this process, nucleation of $NiCo_2O_4$ particles, which lead to nanorod structures, occurred directly on the active surface of the Ni felt, achieving a catalyst loading of approximately 5 mg/cm^2, which is confirmed by weighing the bare Ni Felt before sono-hydrothermal reaction and after calcination. This so-produced electrode is hereafter named NiCo-D.

2.3. Spray-Coating Preparation of the Electrode. The spray coating method was selected as an established and widely known technique for the fabrication of electrodes for AEM-WE.[4,33,35−37] The $NiCo_2O_4$ ink was prepared by mixing the catalyst powders with Aemion+ AF3-HWK9-75-X ionomer (for AEM-WE) or Nafion binder (for AEL, to withstand strongly alkaline media) in an

https://doi.org/10.1021/acsaem.5c01487
ACS Appl. Energy Mater. XXXX, XXX, XXX−XXX

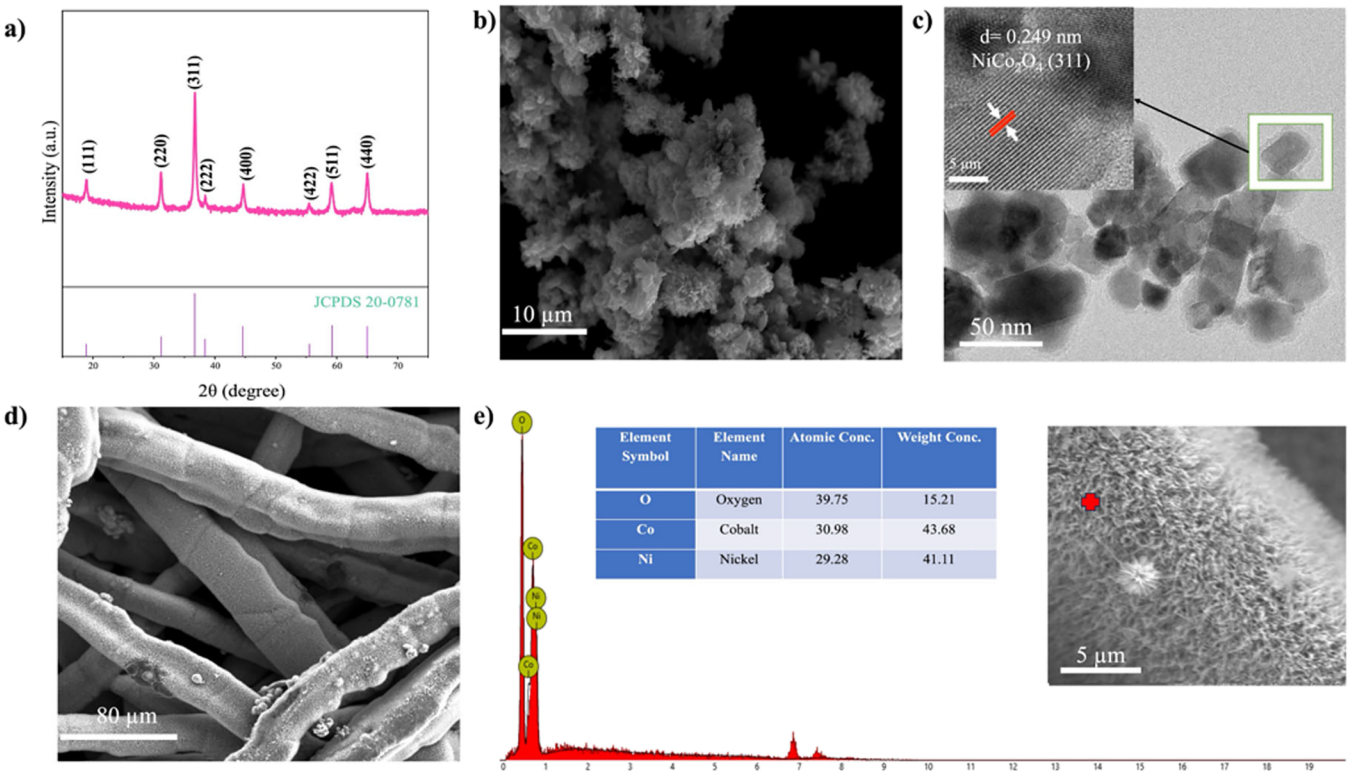

Figure 2. Physicochemical characterization of materials: (a) XRD of $NiCo_2O_4$. (b) SEM of $NiCo_2O_4$ collected on the powder sample obtained by the sono-hydrothermal method. (c) TEM image collected on the powder $NiCo_2O_4$ sample obtained by the sono-hydrothermal method. (d) SEM image and (e) EDS spectrum and related image (spectrum collected in the red spot), on the pristine NiCo-D electrode.

EtOH:water mixture 1:1,[38] using a catalyst concentration from 2 to 5 g/L and ionomer concentration from 0.2 to 1 g/L,[31] i.e., in the optimal ranges suggested by Faid et al.[39] The dispersion was then homogenized by sonication for 1 h before use. The catalyst ink was sprayed using a spray gun with a 0.5 mm nozzle (FE-134K aerograph plus FD-186 compressor, Fengda, operated at 1.5 bar with compressed air) onto the Ni felt, with the substrates placed on a hot plate at 80 °C.[39,40] The amount of deposited catalyst was controlled by weighing the electrodes before and after catalyst deposition until reaching a catalyst loading of 5 mg/cm^2 to have the same loading as that of the direct-grown electrode NiCo-D, and the electrode is hereafter named NiCo-S. The catalyst load was the same for both directly grown and sprayed ones.

The Pt/C inks, used for the preparation of cathodes, were prepared similarly to the $NiCo_2O_4$ ones and adjusting the ionomer concentration as suggested in the work of Koch et al.,[31] ranging from 0.2 to 0.3 g/L. The Pt mass loading was 0.5 mgPt/cm^2, compliant with standard low PGM cathodes.[41,42]

2.4. Physicochemical Characterization of Materials. Various analytical techniques were used to thoroughly investigate the physical and chemical properties of the materials. X-ray diffraction (XRD) measurements were conducted using a PANalytical AERIS diffractometer, allowing analyzing the crystal structure and phase purity of the samples. The morphology of the samples was investigated with a TESCAN scanning electron microscope (SEM), which is coupled with energy-dispersive spectroscopy (EDS) was utilized to determine both the distribution and elemental composition of the materials and electrodes used in this study. Additionally, transmission electron microscopy (TEM) was performed with a JEM 2100 Plus instrument from JEOL Ltd. (Japan) to reveal the morphology and structure of the NiCo2O4 powder.

2.5. Evaluation of Electrochemical Performances. Three-electrode cell measurements were performed using an IVIUM Vertex 10A potentiostat workstation (Ivium Technologies B.V., Netherlands), and a 1 M aqueous KOH was used as the electrolyte. The working electrodes (1 cm × 1 cm) included NiCo-S, NiCo-D, and Ni felt (the latter representing the operative blank). A Hg/HgO, filled with a 1 M KOH solution, was used as the reference electrode, while the counter electrode was a Pt foil (0.5 mm ID, BAS, Japan). All the potentials reported in the paper are converted to the RHE scale and corrected by the ohmic drop of the system by usingeq 1:

$$E(\mathrm{RHE}) = E_{\mathrm{Hg/HgO}} + 0.927\ \mathrm{V} - iR_{\mathrm{uc}} \quad (1)$$

where R_{uc} is the series resistance calculated from EIS.[43,44] Polarization curves were recorded through backward linear sweep voltammetry (LSV) in the range of 1.0 to 1.7 V vs RHE at a potential scan rate of 5 mV/s for better estimation of the OER overpotentials and activity. Backward LSV allows avoiding the influence of oxidation state changes that typically occur during the forward scan, which can affect the accurate determination of overpotentials at lower current densities (e.g., 10 mA cm^{-2}). Electrochemical impedance spectroscopy (EIS) was performed across a frequency range of 0.01 to 100,000 Hz at a potential of 0.55 V vs Hg/HgO. The obtained spectra were matched and fitted with the proper equivalent circuit (represented mostly by $R(RQ)$) to regress R_{uc}.

A VMP3 potentiostat (Biologic, France) equipped with an external 20 A booster channel and an external EIS channel was used to power water electrolyzer single cells, performing galvanostatic polarization curves and EIS measurements. Polarization curves were collected galvanostatically according to a stepwise chronopotentiometric approach. The current density window investigated ranged from 50 mA cm^{-2} to 2 A cm^{-2}, with each step lasting 3 min. $I-V$ data were obtained by averaging the cell voltage obtained from the last minute of each step. High-frequency resistance (HFR), associated with the separator resistance from the intercept of the Nyquist plot with the real axis at 100,000 Hz, was recorded to evaluate the change in MEA. It is important to note that all the data for the cells (AEL and AEM-WE) are presented without i × HFR correction, reflecting the practical operating conditions typically encountered in industrial applications. No HFR correction was applied to the zero-gap cell, as these tests were designed to reflect industrially relevant conditions

https://doi.org/10.1021/acsaem.5c01487
ACS Appl. Energy Mater. XXXX, XXX, XXX−XXX

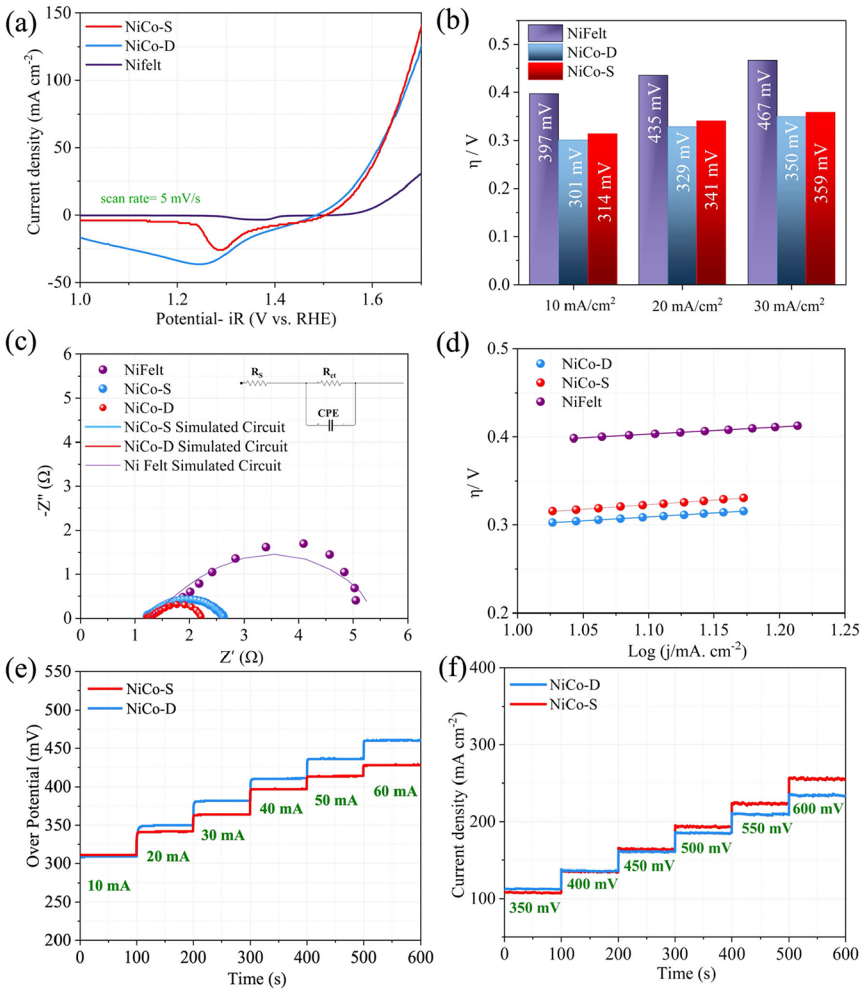

Figure 3. Three-electrode cell configuration measurements for NiCo-D, NiCo-S, and Ni felt: (a) backward LSV scans, with 5 mV/s scan rate (b) comparison of the OER overpotentials measured for the electrodes at different current densities. (c) Electrochemical impedance spectroscopy (EIS) analysis and (d) pseudo-Tafel plots for the investigated electrodes. (e) Chronopotentiometry (CP) and (f) chronoamperometry (CA) tests were collected at different current and potentials (CP and CA reported without iR_{uc} correction).

where ohmic losses, mainly from MEA, are intrinsic to the system. In contrast, *iR* correction was applied to the three-electrode measurements, following standard practice in electrocatalysis, to more accurately assess the intrinsic activity and stability of the catalysts.

2.6. AEL and AEM-WE Single Cell Assembly. The AEL and AEM-WE (with an active area of 5 cm^2) single cells were assembled using the zero-gap cell fixture produced by Antares Electrolysis (Italy), which includes corrosion-resistant Ni anodic plates equipped with flow fields and Ethylene-Propylene Diene Monomer O-ring seals. The cell components, including the separator (Zirfon Perl UTP 220 diaphragm for AEL and Aemion+ AF3-HWK9-75-X for AEM-WE) and electrodes, were compressed to achieve zero-gap cell configurations. In the case of AEM-WE cells, the assembly was performed using activated and hydrated AEMs to prevent cracking and damage to the membranes.[45] Moreover, the membrane is activated by placing it inside the 1 M KOH for at least 24 h. For each electrode compartment, polytetrafluoroethylene spacers were used to ensure proper compression of the cathode/AEM/anode stack (i.e., the MEA). The spacer thickness was optimized to ensure a GDL compression of about 15% ± 5%. Sprayed Pt/C electrodes were used as cathodes, while NiCo-D or NiCo-S were used as anodes, and all electrodes, before mounting inside the cell, were kept in 1 M KOH for at least 30 min. The cells were operated differently depending on the separator used. AEL cells were operated at 80 °C using 30 wt % aqueous KOH as electrolyte, flowing at both anode and cathode. Two different reservoirs were used for the anolyte and catholyte, both flowed at 5 mL min^{-1}. AEM-WE cells were operated at 60 °C using 1 M aqueous KOH as electrolyte in dry cathode mode. Therefore, the electrolyte was fed only to the anode with a flow rate of 5 mL min^{-1}. Both types of cells were operated in a two-electrode configuration. For AEM-WE, Aemion+ AF3-HWK9-75-X ionomer is used as the binder for spraying Pt/C on the cathode as well as NiCo-S on the anode. For AEL, the Pt/C is sprayed using Nafion binder (with a binder to catalyst weight of 2:10), corresponding to a weight ratio. Nafion is used for spraying AEL's cathode since it is adopted for AEL at an industrial scale, due to its good stability and lower cost than that of the anionic binders.

3. RESULTS AND DISCUSSION

3.1. Physicochemical Characterization of Materials. The XRD, SEM, EDS, and TEM characterizations were performed to evaluate the physicochemical properties of the synthesized materials and electrodes, as shown in Figure 2.

Figure 2a shows the XRD pattern of the synthesized $NiCo_2O_4$ powder within the 2θ range of 20° to 80°. According to JCPDS No-20-0781, the peaks observed at 18.90°, 31.15°, 36.70°, 38.40°, 44.62°, 55.43°, 59.09°, 64.98°, and 77.54° correspond to the (111), (220), (311), (222), (400), (422), (511), (440), and (533) crystallographic planes, respectively, confirming the cubic structure of $NiCo_2O_4$.[46] The sharp, well-defined peaks indicate high crystallinity, meaning that the

https://doi.org/10.1021/acsaem.5c01487
ACS Appl. Energy Mater. XXXX, XXX, XXX−XXX

sono-hydrothermal method combined with calcination fosters optimal nucleation of the electrocatalyst. This is further corroborated by SEM and TEM analyses of the $NiCo_2O_4$ powder, as shown in Figure 2b,c, respectively. Figure 2b displays an SEM image revealing a mum-flower-like structure, where the $NiCo_2O_4$ rods cluster together. The TEM analysis in Figure 2c reveals particle sizes in the range from 20 to 45 nm. Additionally, the lattice spacing (d) of 0.249 nm, associated with the (311) plane of $NiCo_2O_4$ spinel, validates the successful synthesis via the sono-hydrothermal method, with urea serving as the hydrolysis agent.[47]

The electrode fabricated using the direct growth method (NiCo-D) was investigated through SEM and EDS measurements, as reported in Figure 2d,e, respectively. Figure 2d reveals a homogeneous growth of $NiCo_2O_4$ electrocatalyst across the Ni felt fibers while maintaining the porosity of the electrode and preventing blockage of the pore sites. The rod-like structure of the electrocatalyst, together with its nanostructuring, provides a large surface area, aiming at enhancing electrochemical reaction kinetics.[48,49] The EDS analysis in Figure 2e further confirms the purity of $NiCo_2O_4$ and aligns with the expected stoichiometry of the spinel structure. The use of urea as a hydrolysis agent, combined with the sonothermal synthesis method, enables the formation of small $NiCo_2O_4$ nuclei. These nuclei grow homogeneously not only on the surface of the activated Ni felt but also inside the pores (the detail in Figure 2e shows the single fiber of NiFelt with NiCo-D grown on it), ensuring an even distribution of Ni^{2+} and Co^{2+} ions and contributing to the electrochemical activity of the electrocatalyst; however the presence of electrocatalyst is limited at the bottom of the GDL (Figure S7 in SI).[50,51]

Overall, XRD, SEM, and TEM analyses confirm the successful synthesis of the $NiCo_2O_4$ spinel electrocatalyst via the sonothermal method using urea as a hydrolysis agent. XRD demonstrates high crystallinity, while SEM and TEM analysis reveal mum-flower-like rod structures with high purity.

3.2. Assessment of Electrodes OER Performance in a Standard Three-Electrode Setup. Three-electrode cell configuration experiments were carried out on NiCo-D, NiCo-S, and bare Ni felt to preliminarily assess their catalytic activity for the OER before being moved to industrially relevant AEL or AEM-WE testing in a two-electrode flow cell configuration.

Figure 3a reports the 100% iR_{uc}-corrected LSV curve, acquired using the backward potential scan mode. NiCo-S, NiCo-D, and Ni felt achieved a current density of 10 mA cm^{-2} at 1.544, 1.531, and 1.627 V vs RHE, which corresponds to 314, 301, and 397 mV of overpotentials (Figure 3b), respectively. Clearly, the presence of $NiCo_2O_4$ on the surface of Ni felt significantly improves the electrochemical activity of the bare support, regardless of the electrode fabrication method (i.e., whether a binder is used or not). Tentatively, this higher activity of the freestanding NiCo-D electrode is ascribed to the absence of the binder in the catalyst layer, resulting in a higher number of OER active sites exposed to the electrolyte.

As shown in Figure 3c, Nyquist plots were fit using an electrical equivalent circuit, shown in the inset panel. Here, R_{uc} is the uncompensated resistance of the system, at high frequencies (~1.23 Ω at 100 kHz for all of the investigated electrodes extracted from the equivalent fitted circuit), and R_{ct} is the charge transfer resistance, corresponding to the diameter of the semicircles. Estimated R_{ct} are 1.38, 0.996, and 3.53 Ω for NiCo-S, NiCo-D, and Ni felt, respectively. Consistent with previous results and considerations, the lower R_{ct} is measured for the freestanding NiCo-D electrode, for which the electrocatalyst is directly grown on the Ni felt in the absence of any ionomer/binder, thus facilitating the transfer of electrons. On the other hand, the NiCo-S, which is fabricated by spraying an electrocatalyst ink (containing a 1:10 solid weight ratio of binder to catalyst inside the ink) on the surface of the Ni felt, displays a higher R_{ct}.

Figure 3d shows the pseudo-Tafel slopes for NiCo-S, NiCo-D, and Ni felt extracted from LSV with a 5 mV/s scan rate and a 2 mV step, providing key information about the OER kinetics of the electrodes (the description of pseudo-Tafel slopes is provided in the SI). The slopes measured for NiCo-S, NiCo-D, and Ni felt are 84.1, 79.7, and 130.4 mV/dec, respectively, consistently demonstrating that NiCo-D exhibits enhanced OER kinetics with respect to the other electrodes. It is also noteworthy that the presence of $NiCo_2O_4$ on the support results in a significant enhancement of its electrochemical activity compared with bare Ni felt.

The OER activity of both NiCo-S and NiCo-D was further evaluated by means of either chronopotentiometry (CP) or chronoamperometry (CA) protocols, also aimed at a preliminary assessment of their stability. In the CP and CA test (Figure 3e,f), both protocols consistently indicate that NiCo-D performs better at low current densities while NiCo-S works better at higher current densities, consistent with the LSV. This behavior could be attributed to a slightly different gas bubble removal capability of the two electrodes, more noticeable at higher current densities for gas bubble detachment (the catalyst layer on NiCo-D is in a 3D structure, while in NiCo-S the catalyst is present only on the surface, due to spraying on GDL). These data highlight once more how an electrocatalyst, deemed the most promising from most three-electrode testing at lab-scale, might turn out to be less performant under industrially relevant conditions, for example, when required to operate at high current densities. With the aim of validating our electrodes in a real industrial scenario, we then proceeded to test them in flow cells under both AEL and AEM configurations.

3.2.1. AEL Test of the Direct-Growth Anode. Binder-free electrodes offer significant advantages for AELs, particularly in terms of durability and efficiency.[52] By eliminating binders, which can degrade in harsh alkaline environments, these electrodes reduce the risk of catalyst detachment and ensure long-term stability. Moreover, the direct integration of the catalyst into the substrate enhances electrical conductivity by providing uninterrupted pathways for electron transfer, optimizing the performance. Additionally, binder-free designs simplify manufacturing processes, lowering costs and making them more suitable for large-scale applications. Based on these considerations, NiCo-D was first tested as an anode in a 5 cm^2 zero-gap AEL single cell fed with 30 wt % KOH aqueous electrolyte and operating at 80 °C. A Pt/C electrode (see the Methods section for details) was used as a benchmark cathode. At first, the full cell underwent an activation procedure (mainly needed to condition the diaphragm and the electrodes but also to allow for the thermalization of the overall system), which is reported and commented in the Supporting Information, Figure S1. Briefly, the $I-V$ curve of the cell stabilizes in the last 30−40 min of the activation process (ca. 3 h long), with the cell voltage plateauing at ca. 1.78 V (@ 1 A cm^{-2}) and the

https://doi.org/10.1021/acsaem.5c01487
ACS Appl. Energy Mater. XXXX, XXX, XXX−XXX

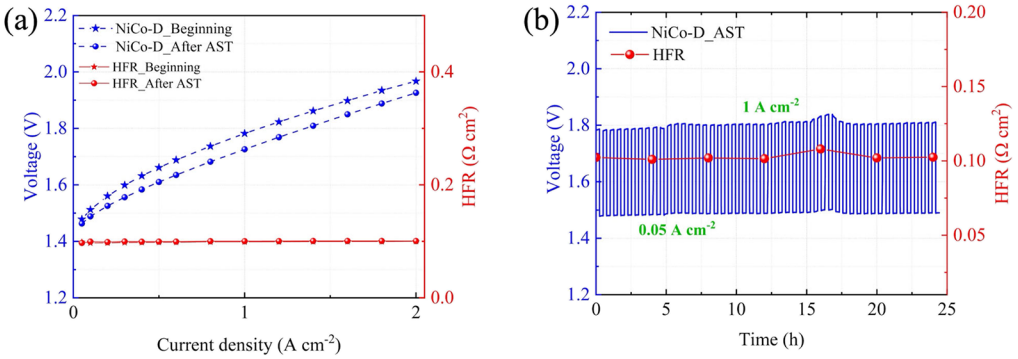

Figure 4. Characterization of a single cell AEL implementing NiCo-D as the anode: (a) Galvanostatic polarization curves (and HFR from EIS at each galvanostatic step) collected before (stars) and after (circles) the AST. (b) 24-h-long AST.

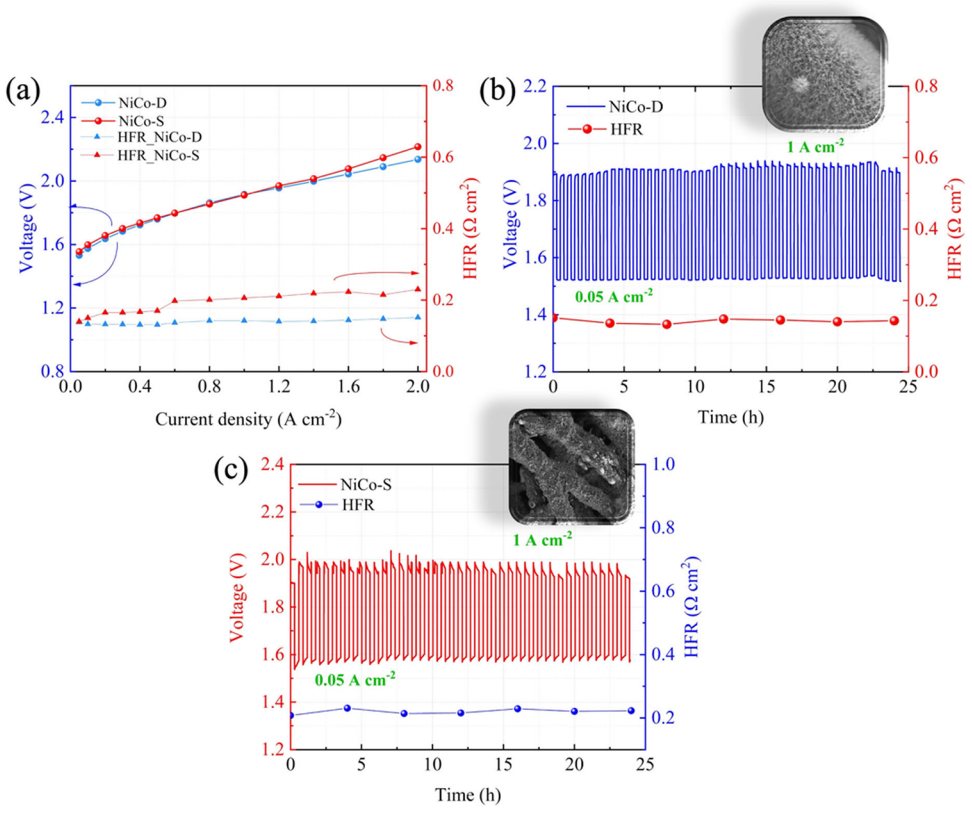

Figure 5. AEM-WE characterization. (a) Polarization curves and HFR collected on NiCo-D and NiCo-S before AST. Electrochemical traces obtained from AST on (b) NiCo-D and (c) NiCo-S.

HFR of the system reaching a stable minimum value at ca. 0.1 Ω cm^2. The activation was followed by the collection of a galvanostatic polarization curve (blue stars in Figure 4a), a 24 h long CP step at 1 A cm^{-2} (Figure S2), a 24 h accelerated stress test (AST, Figure 4b), and a final galvanostatic polarization curve (blue circles in Figure 4a). The initial polarization curve demonstrates that the AEL implementing NiCo-D achieves state-of-the-art performance, delivering 1 and 2 A cm^{-2} at 1.78 and 1.96 V, respectively. The stability of the performance at 1 A cm^{-2} is confirmed by the day-long CP registered afterward, with minimal potential oscillation, mainly imputable to electrolyte refilling operations and temperature variations in the lab (Figure S2, blue curve). Consistently, the HFR (red circles in Figure S2) is stable and low throughout the whole experiment. The AST corroborates the stability data, demonstrating that the cell can withstand harsh load variations (cycling from 1 A cm^{-2} to 50 mA cm^{-2} every 15 min for 24 h) and thus is, in principle, compatible with renewable energy sources. It is noteworthy that the AEL cell not only maintained this performance after the AST (post-AST polarization curve, Figure 4a, blue circles) but also achieved better performances, showing 1.73 V at 1 A cm^{-2} and 1.92 V at 2 A cm^{-2}. Such an increase is tentatively ascribed to the roughening of the electrode under harsh alkaline and anodic conditions, leading to an increase in the physical and electrochemically active surface area. Overall, these results highlight the remarkable OER activity of the NiCo-D electrodes and the stability of the present AEL cell configuration and the embedded catalysts.

3.2.2. AEM-WE Test of Direct-Growth and Spray-Coated Anodes. In AELs, binder-free electrodes are highly valued for their simplicity and stability. However, under the AEM-WE configuration, electrodes require the presence of ionomers in

https://doi.org/10.1021/acsaem.5c01487
ACS Appl. Energy Mater. XXXX, XXX, XXX−XXX

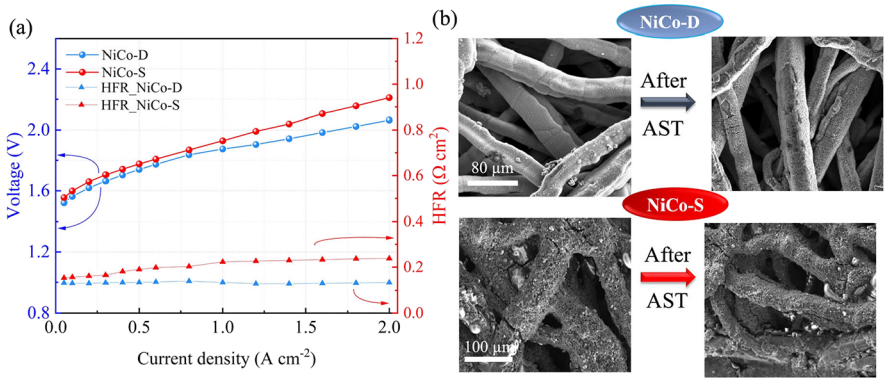

Figure 6. AEM-WE characterization after the AST: (a) polarization curve and HFR of NiCo-D and NiCo-S. (b) SEM images comparing NiCo-D and NiCo-S before and after operation.

the catalyst layer to ensure ionic continuity and thus achieve optimal performance. Nonetheless, ionomers can reduce the electrode activity by blocking access to active sites. Currently, the role of ionomers in AEM-WEs is still under study.[20,53] Although binder incorporation in the cathode layer is paramount in AEM-WE operated in dry cathode mode, there are markedly fewer investigations dedicated to shedding light on the importance of ionomers in the anodic catalyst layer.

In order to investigate this matter, NiCo-D and NiCo-S electrodes were used as anodes in atmospheric pressure AEM-WE single cells fed with 1 M KOH and operating at 60 °C in a dry cathode configuration. Pt/C electrodes (using Aemion+ AF3-HWK9-75-X as ionomer) served as benchmark cathodes. Cells were named after their respective anodes. Both cells underwent the same electrochemical routine reported for the AEL configuration. It is important to point out that, in the case of AEM-WEs, the activation procedure (Figure S3 and related discussion) is fundamental to properly hydrate and condition the AEM itself and is indeed generally recommended by the producers. Figure 5a shows the initial polarization curves (and HFR measured at the end of each current step) for NiCo-D (blue) and NiCo-S (red). The traces obtained from the two cells are almost juxtaposed, with a divergence only at current densities higher than 1.5 A cm^{-2}, over which NiCo-D performs slightly better than its sprayed counterpart. Interestingly, the HFR of the cell implementing NiCo-S (i.e., the electrode in which the ionomer is present in the catalyst layer) is higher than that recorded for NiCo-D. These results suggest that the presence of the ionomer in the anodic catalyst layer might not be fundamental for the good functioning of an AEM-WE operated with 1 M KOH anolyte. 24 h long CP at 1 A cm^{-2}, collected on both cells (Figures S4a and S5a) return consistent results, while post-CP polarization curves (Figures S4b and S5b) confirm the stability of both systems. The electrochemical traces obtained from the AST conducted on both cells are reported in Figure 5b,c. In accordance with fixed current stability tests (Figures S4 and S5), AST demonstrates the robustness of both systems and their similar voltage performance. Similarly, the lower HFR of the deposited electrode is confirmed.

Post-AST polarization curves (Figure 6a) are consistent with the initial curves, further corroborating the stable performance of the overall electrochemical system. Focusing on anode stability, Figure 6b reports the before and after AST SEM images of both NiCo-D and NiCo-S. For NiCo-D, most nanorods remained intact on the Ni-felt substrate, with some detachment observed (Figure S6, Supporting Information), likely occurring during disassembly, as parts adhered to the membrane. NiCo-S displayed a similar scenario, indicating that the direct growth method produces results comparable to those achieved with the use of binders regarding catalyst adhesion to the electrode surface. The homogeneity of the catalyst layer is preserved on both electrodes, despite a slight roughening of the surface may be qualitatively observed.

When it comes to similar electrodes in this content, the results of both NiCo-D and NiCo-S with 5 mg·cm^{-2} of loading seem reliable for AEM-WE. For instance, Ahmed et al. used the $NiCo_2O_4$ deposited on the nickel foam (25 mg·cm^{-2} of loading) as anode, 1 mg·cm^{-2} of Pt loading on carbon paper in combination with the dioxide membrane Sustainion X-37-50 (grade T with a thickness of 50 μm), which achieved approximately 2.1 V at 1 A·cm^{-2} at 55 °C with 1 M KOH.[54] Moreover, Cossar et al. which focused on the role of ionomer in the performance of electrode and AEM-WE revealed that the $Ni_{90}Fe_{10}$ catalyst with 5 mg·cm^{-2} of loading on gold (Au)-coated titanium (Ti) felt (2GDL20-1,0, 1 mm thick, Bekaert Corporation, Marietta, GA) in combination with 1 mg·cm^{-2} of Pt/C loading on Teflon-treated carbon paper with Aemion AF1-HNN8-50-X membrane achieved 1.941 V at 0.4 A·cm^{-2}.[37]

4. CONCLUSIONS

In this study, we successfully tested a $NiCo_2O_4$ catalyst, modified in morphology using the sono-hydrothermal method, for applications in both AELs and AEM-WEs. Physicochemical analyses, including SEM and TEM, confirmed the nanorod-like structure of the catalyst, which enhances electrochemical activity and improves conductivity. These findings were further supported by three-electrode cell measurements.

Using innovative fabrication methods, we demonstrated the effectiveness of direct-grown $NiCo_2O_4$ electrodes as binder-free solutions for AELs, achieving an outstanding performance (cell voltage of 1.78 V at 1 A cm^{-2}). Additionally, we compared the binder-free $NiCo_2O_4$ electrodes with their spray-coated counterparts incorporating ionomers in AEM-WE systems. Both electrode types exhibited promising performances (1.915 V vs 1.911 V at 1 A cm^{-2} after preconditioning) and durability, as validated by 24-h fixed current stability tests followed by 24-h accelerated stress tests.

The binder-free approach, which yielded excellent results in AELs, is therefore also a promising methodology for AEM-WEs, especially considering the safety and environmental

https://doi.org/10.1021/acsaem.5c01487
ACS Appl. Energy Mater. XXXX, XXX, XXX−XXX

benefits of avoiding nanometric powder spraying during electrode fabrication. These results also highlight the versatility, scalability, and sustainability of $NiCo_2O_4$-based electrodes for advanced electrolyzer technologies. Although optimizing ionomer and catalyst loading on the electrode surface by spraying may provide further performance improvements, paving the way for more efficient large-scale electrolyzer applications compared to current designs of AEMWEs and AELs, this preliminary study indicates that the use of directly grown (i.e., binder-free) anodes may represent an efficient platform under both AEL and AEM-WE configurations.

■ ASSOCIATED CONTENT

Supporting Information

The Supporting Information is available free of charge at https://pubs.acs.org/doi/10.1021/acsaem.5c01487.

Figure S1: voltage and HFR during AEL activation; Figure S2: AEL fixed load stability test; Figure S3: AEM-WE activation; Figure S4: NiCo-D AEM-WE electrochemical stability and performance; Figure S5: NiCo-S AEM-WE electrochemical stability and performance; Figure S6: SEM analysis of NiCo-D single fiber after test in AEM-WE; and Figure S7: SEM image of the bottom surface of the Ni felt after NiCo-D deposition (PDF)

■ AUTHOR INFORMATION

Corresponding Author

Ombretta Paladino − *Department of Civil, Chemical and Environmental Engineering (DICCA), Università di Genova, 16145 Genoa, Italy;* orcid.org/0000-0003-1111-7944; Email: paladino@unige.it

Authors

Ataollah Niyati − *Department of Civil, Chemical and Environmental Engineering (DICCA), Università di Genova, 16145 Genoa, Italy;* orcid.org/0009-0006-5233-9649

Arianna Moranda − *Department of Civil, Chemical and Environmental Engineering (DICCA), Università di Genova, 16145 Genoa, Italy*

Sebastiano Bellani − *Antares Electrolysis S.r.l., 16121 Genova, Italy*

Thi Hong Hanh Le − *Nanochemistry Department, Istituto Italiano di Tecnologia (IIT), 16163 Genova, Italy*

Michele Ferri − *Antares Electrolysis S.r.l., 16121 Genova, Italy; Nanochemistry Department, Istituto Italiano di Tecnologia (IIT), 16163 Genova, Italy*

Complete contact information is available at: https://pubs.acs.org/10.1021/acsaem.5c01487

Author Contributions

A.N.: conceptualization, methodology, investigation, formal analysis, writing original draft, data curation. A.M.: writing, review and editing, methodology. S.B.: writing original draft, validation, methodology, investigation, formal analysis, data curation. T.H.H.L.: writing, review and editing, investigation, data curation. M.F.: writing, review and editing. O.P.: conceptualization, methodology, writing-original draft, validation, supervision, project administration, funding acquisition.

Funding

This work is partially funded by NextGeneration EU, PNRR project, M2C213.5, NEMESI: Nuovi Elettrodi e Membrane per Elettrolizzatori a Scala Industriale, ID: RSH2B_000002, CUP: F39J22001960004. A.N. is supported by a PhD grant FSE+2021-2027, ESO 4.6.

Notes

S.B. and M.F. are among the cofounder and currently serve as CTO and CSO, respectively, of Antares Electrolysis, a company developing and commercializing AEM electrolyzer stacks.

The authors declare no competing financial interest.

■ ACKNOWLEDGMENTS

The authors wish to thank Prof. Antonio Comite (Head of the Elemental lab at DCCI, Department of Chemistry of the University of Genoa) and Mrs. Laura Negretti, who carried out TEM analyses at DCCI; Dr. Juan F. Basbus, who carried out XRD analyses at DICCA.

■ REFERENCES

(1) Campo Schneider, L. P.; Dhrioua, M.; Ullmer, D.; Egert, F.; Wiggenhauser, H. J.; Ghotia, K.; Kawerau, N.; Grilli, D.; Razmjooei, F.; Ansar, S. A. Advancements in Hydrogen Production Using Alkaline Electrolysis Systems: A Short Review on Experimental and Simulation Studies. *Curr. Opin Electrochem* **2024**, *47*, No. 101552.

(2) Afanasev, P.; Askarova, A.; Alekhina, T.; Popov, E.; Markovic, S.; Mukhametdinova, A.; Cheremisin, A.; Mukhina, E. An Overview of Hydrogen Production Methods: Focus on Hydrocarbon Feedstock. *Int. J. Hydrogen Energy* **2024**, *78*, 805−828.

(3) Hassan, Q.; Algburi, S.; Sameen, A. Z.; Salman, H. M.; Jaszczur, M. Green Hydrogen: A Pathway to a Sustainable Energy Future. *Int. J. Hydrogen Energy* **2024**, *50*, 310−333.

(4) Khataee, A.; Shirole, A.; Jannasch, P.; Krüger, A.; Cornell, A. Anion Exchange Membrane Water Electrolysis Using Aemion™ Membranes and Nickel Electrodes. *J. Mater. Chem. A Mater.* **2022**, *10* (30), 16061−16070.

(5) Klingenhof, M.; Selve, S.; Günther, C. M.; Schmidt, J.; Razmjooei, F.; Strasser, P.; Ansar, S.-A. All Platinum-Group-Metal-Free Alkaline Exchange Membrane Water Electrolyzers Using Direct Hydrothermal Catalyst Deposition on Raney Ni Substrate. *ACS Appl. Energy Mater.* **2024**, *7* (16), 6856−6861.

(6) Lira Garcia Barros, R.; Kelleners, M. H. G.; van Bemmel, L.; van der Leegte, T. V. N.; van der Schaaf, J.; de Groot, M. T. Elucidating the Increased Ohmic Resistances in Zero-Gap Alkaline Water Electrolysis. *Electrochim. Acta* **2024**, *507*, No. 145161.

(7) Kim, Y.; Jung, S.-M.; Kim, K.-S.; Kim, H.-Y.; Kwon, J.; Lee, J.; Cho, H.-S.; Kim, Y.-T. Cathodic Protection System against a Reverse-Current after Shut-Down in Zero-Gap Alkaline Water Electrolysis. *JACS Au* **2022**, *2* (11), 2491−2500.

(8) Jung, S.; Kim, Y.; Lee, B.; Jung, H.; Kwon, J.; Lee, J.; Kim, K.; Kim, Y.; Kim, K.; Cho, H.; Park, J. H.; Han, J. W.; Kim, Y. Reverse-Current Tolerance for Hydrogen Evolution Reaction Activity of Lead-Decorated Nickel Catalysts in Zero-Gap Alkaline Water Electrolysis Systems. *Adv. Funct. Mater.* **2024**, *34* (27), No. 2316150.

(9) Amireh, S. F.; Heineman, N. N.; Vermeulen, P.; Barros, R. L. G.; Yang, D.; van der Schaaf, J.; de Groot, M. T. Impact of Power Supply Fluctuation and Part Load Operation on the Efficiency of Alkaline Water Electrolysis. *J. Power Sources* **2023**, *560*, No. 232629.

(10) Kang, S.; Kim, Y.; Wilke, V.; Bae, S.; Chmielarz, J. J.; Sanchez, D. G.; Ham, K.; Gago, A. S.; Friedrich, K. A.; Lee, J. Stabilizing Pure Water-Fed Anion Exchange Membrane Water Electrolyzers through Membrane−Electrode Interface Engineering. *ACS Appl. Mater. Interfaces* **2024**, *16* (36), 47387−47395.

(11) de Groot, M. T.; Vreman, A. W. Ohmic Resistance in Zero Gap Alkaline Electrolysis with a Zirfon Diaphragm. *Electrochim. Acta* **2021**, *369*, No. 137684.

(12) Zhu, J.; Chen, W.; Poli, S.; Jiang, T.; Gerlach, D.; Junqueira, J. R. C.; Stuart, M. C. A.; Kyriakou, V.; Costa Figueiredo, M.; Rudolf, P.; Miola, M.; Morales, D. M.; Pescarmona, P. P. Nanostructured Fe-Doped Ni_3S_2 Electrocatalyst for the Oxygen Evolution Reaction

with High Stability at an Industrially-Relevant Current Density. *ACS Appl. Mater. Interfaces* **2024**, *16* (43), 58520−58535.
(13) Chen, B.; Mardle, P.; Holdcroft, S. Probing the Effect of Ionomer Swelling on the Stability of Anion Exchange Membrane Water Electrolyzers. *J. Power Sources* **2022**, *550*, No. 232134.
(14) Moradizadeh, L.; Madhavan, P. V.; Chellehbari, Y. M.; Gupta, A.; Li, X.; Shahgaldi, S. Porous Transport Layers with Low Pt Loading Having Nb−Ta Alloy as Interlayer for Proton Exchange Membrane Water Electrolyzers. *Int. J. Hydrogen Energy* **2024**, *94*, 1114−1129.
(15) Kang, Z.; Chen, Y.; Wang, H.; Alia, S. M.; Pivovar, B. S.; Bender, G. Discovering and Demonstrating a Novel High-Performing 2D-Patterned Electrode for Proton-Exchange Membrane Water Electrolysis Devices. *ACS Appl. Mater. Interfaces* **2022**, *14* (1), 2335−2342.
(16) Falqueto, J. B.; Hales, N.; Schimidt, T. J.; Fabbri, E. Recent Advances in Nickel-Based Perovskite Oxides for the Electrocatalytic Oxygen Evolution Reaction in Alkaline Electrolytes. *ACS Mater. Lett.* **2024**, *6*, 5227−5241.
(17) Galkina, I.; Faid, A. Y.; Jiang, W.; Scheepers, F.; Borowski, P.; Sunde, S.; Shviro, M.; Lehnert, W.; Mechler, A. K. Stability of Ni−Fe-Layered Double Hydroxide Under Long-Term Operation in AEM Water Electrolysis. *Small* **2024**, *20* (26), No. 2311047.
(18) Klingenhof, M.; Trzesniowski, H.; Koch, S.; Zhu, J.; Zeng, Z.; Metzler, L.; Klinger, A.; Elshamy, M.; Lehmann, F.; Buchheister, P. W.; Weisser, A.; Schmid, G.; Vierrath, S.; Dionigi, F.; Strasser, P. High-Performance Anion-Exchange Membrane Water Electrolysers Using NiX (X = Fe,Co,Mn) Catalyst-Coated Membranes with Redox-Active Ni−O Ligands. *Nat. Catal* **2024**, *7* (11), 1213−1222.
(19) Mayerhöfer, B.; McLaughlin, D.; Böhm, T.; Hegelheimer, M.; Seeberger, D.; Thiele, S. Bipolar Membrane Electrode Assemblies for Water Electrolysis. *ACS Appl. Energy Mater.* **2020**, *3* (10), 9635−9644.
(20) Hyun, J.; Hwan Yang, S.; Wook Lee, D.; Oh, E.; Bae, H.; Suc Cha, M.; Doo, G.; Yong Lee, J.; Kim, H.-T. Impact of the Binding Ability of Anion Exchange Ionomer on the Initial Performance Degradation of Anion Exchange Membrane Water Electrolyzers. *Chemical Engineering Journal* **2023**, *469*, No. 143919.
(21) Chand, K.; Paladino, O. Recent Developments of Membranes and Electrocatalysts for the Hydrogen Production by Anion Exchange Membrane Water Electrolysers: A Review. *Arabian Journal of Chemistry* **2023**, *16* (2), No. 104451.
(22) Mardle, P.; Chen, B.; Holdcroft, S. Opportunities of Ionomer Development for Anion-Exchange Membrane Water Electrolysis. *ACS Energy Lett.* **2023**, *8* (8), 3330−3342.
(23) Omidi-Dargahi, A.; Dehghani, H.; Ehsani, A. Electrochemical Performance of NiCo2O4/Functionalized Graphene Oxide with Phenylalanine and Tryptophane as Efficient Electrodes to Enhance Capacitance Properties in Supercapacitors. *J. Energy Storage* **2024**, *76*, No. 109824.
(24) Kannangara, Y. Y.; Karunarathne, S.; Wijesinghe, W. P. S. L.; Sandaruwan, C.; Ratwani, C. R.; Kamali, A. R.; Abdelkader, A. M. The Electrochemical Performance of Various NiCo2O4 Nanostructures in Hybrid Supercapacitors: Investigating the Impact of Crystalline Defects. *J. Energy Storage* **2024**, *84*, No. 110717.
(25) Perroni, P. B.; Ferraz, T. V. B.; Rousseau, J.; Canaff, C.; Varela, H.; Napporn, T. W. Stainless Steel Supported NiCo2O4 Active Layer for Oxygen Evolution Reaction. *Electrochim. Acta* **2023**, *453*, No. 142295.
(26) Shi, H.; Zhao, G. Water Oxidation on Spinel $NiCo_2O_4$ Nanoneedles Anode: Microstructures, Specific Surface Character, and the Enhanced Electrocatalytic Performance. *J. Phys. Chem. C* **2014**, *118* (45), 25939−25946.
(27) Paladino, O.; Niyati, A.; Moranda, A.; Beigzadeh Arough, P.; Marcenaro, B. Engineering Potential Electrocatalysts for Both AEM Electrolyzers and Redox Flow Batteries: Design of Experiments at the Different Scales. *Appl. Therm Eng.* **2025**, *258*, No. 124532.
(28) Niyati, A.; Moranda, A.; Beigzadeh Arough, P.; Navarra, F. M.; Paladino, O. Electrochemical Performance of a Hybrid NiCo2O4@NiFelt Electrode at Different Operating Temperatures and Electrolyte PH. *Energies (Basel)* **2024**, *17* (15), 3703.
(29) Agudosi, E. S.; Abdullah, E. C.; Numan, A.; Mubarak, N. M.; Aid, S. R.; Benages-Vilau, R.; Gómez-Romero, P.; Khalid, M.; Omar, N. Fabrication of 3D Binder-Free Graphene NiO Electrode for Highly Stable Supercapattery. *Sci. Rep* **2020**, *10* (1), 11214.
(30) Wang, L.; Weissbach, T.; Reissner, R.; Ansar, A.; Gago, A. S.; Holdcroft, S.; Friedrich, K. A. High Performance Anion Exchange Membrane Electrolysis Using Plasma-Sprayed, Non-Precious-Metal Electrodes. *ACS Appl. Energy Mater.* **2019**, *2* (11), 7903−7912.
(31) Koch, S.; Heizmann, P. A.; Kilian, S. K.; Britton, B.; Holdcroft, S.; Breitwieser, M.; Vierrath, S. The Effect of Ionomer Content in Catalyst Layers in Anion-Exchange Membrane Water Electrolyzers Prepared with Reinforced Membranes (Aemion+^{TM}). *J. Mater. Chem. A Mater.* **2021**, *9* (28), 15744−15754.
(32) Plevová, M.; Hnát, J.; Žitka, J.; Pavlovec, L.; Otmar, M.; Bouzek, K. Optimization of the Membrane Electrode Assembly for an Alkaline Water Electrolyser Based on the Catalyst-Coated Membrane. *J. Power Sources* **2022**, *539*, No. 231476.
(33) Fortin, P.; Khoza, T.; Cao, X.; Martinsen, S. Y.; Oyarce Barnett, A.; Holdcroft, S. High-Performance Alkaline Water Electrolysis Using Aemion^{TM} Anion Exchange Membranes. *J. Power Sources* **2020**, *451*, No. 227814.
(34) Niyati, A.; Moranda, A.; Basbus, J. F.; Paladino, O. Unlocking the Potential of $NiCo_2O_4$ Nanocomposites: Morphology Modification Based on Urea Concentration and Hydrothermal and Calcination Temperature. *New J. Chem.* **2024**, *48* (24), 11035−11043.
(35) Qiu, C.; Xu, Z.; Chen, F.-Y.; Wang, H. Anode Engineering for Proton Exchange Membrane Water Electrolyzers. *ACS Catal.* **2024**, *14* (2), 921−954.
(36) Park, J. E.; Bae, H. E.; Karuppannan, M.; Oh, K. M.; Kwon, O. J.; Cho, Y.-H.; Sung, Y.-E. Effect of Catalyst Layer Designs for High-Performance and Durable Anion-Exchange Membrane Water Electrolysis. *Journal of Industrial and Engineering Chemistry* **2022**, *109*, 453−460.
(37) Cossar, E.; Murphy, F.; Walia, J.; Weck, A.; Baranova, E. A. Role of Ionomers in Anion Exchange Membrane Water Electrolysis: Is Aemion the Answer for Nickel-Based Anodes? *ACS Appl. Energy Mater.* **2022**, *5* (8), 9938−9951.
(38) Volk, E. K.; Kreider, M. E.; Kwon, S.; Alia, S. M. Recent Progress in Understanding the Catalyst Layer in Anion Exchange Membrane Electrolyzers−Durability, Utilization, and Integration. *EES Catalysis* **2024**, *2* (1), 109−137.
(39) Faid, A. Y.; Xie, L.; Barnett, A. O.; Seland, F.; Kirk, D.; Sunde, S. Effect of Anion Exchange Ionomer Content on Electrode Performance in AEM Water Electrolysis. *Int. J. Hydrogen Energy* **2020**, *45* (53), 28272−28284.
(40) Vincent, I.; Lee, E.-C.; Kim, H.-M. Highly Cost-Effective Platinum-Free Anion Exchange Membrane Electrolysis for Large Scale Energy Storage and Hydrogen Production. *RSC Adv.* **2020**, *10* (61), 37429−37438.
(41) Riemer, M.; Duval-Dachary, S.; Bachmann, T. M. Environmental Implications of Reducing the Platinum Group Metal Loading in Fuel Cells and Electrolysers: Anion Exchange Membrane versus Proton Exchange Membrane Cells. *Sustainable Energy Technologies and Assessments* **2023**, *56*, No. 103086.
(42) Chen, N.; Paek, S. Y.; Lee, J. Y.; Park, J. H.; Lee, S. Y.; Lee, Y. M. High-Performance Anion Exchange Membrane Water Electrolyzers with a Current Density of 7.68 A Cm^{-2} and a Durability of 1000 h. *Energy. Environ. Sci.* **2021**, *14* (12), 6338−6348.
(43) Kawashima, K.; Márquez, R. A.; Son, Y. J.; Guo, C.; Vaidyula, R. R.; Smith, L. A.; Chukwuneke, C. E.; Mullins, C. B. Accurate Potentials of Hg/HgO Electrodes: Practical Parameters for Reporting Alkaline Water Electrolysis Overpotentials. *ACS Catal.* **2023**, *13* (3), 1893−1898.
(44) Kou, T.; Wang, S.; Li, Y. Perspective on High-Rate Alkaline Water Splitting. *ACS Mater. Lett.* **2021**, *3* (2), 224−234.

https://doi.org/10.1021/acsaem.5c01487
ACS Appl. Energy Mater. XXXX, XXX, XXX−XXX

(45) Xu, D.; Stevens, M. B.; Cosby, M. R.; Oener, S. Z.; Smith, A. M.; Enman, L. J.; Ayers, K. E.; Capuano, C. B.; Renner, J. N.; Danilovic, N.; Li, Y.; Wang, H.; Zhang, Q.; Boettcher, S. W. Earth-Abundant Oxygen Electrocatalysts for Alkaline Anion-Exchange-Membrane Water Electrolysis: Effects of Catalyst Conductivity and Comparison with Performance in Three-Electrode Cells. *ACS Catal.* **2019**, *9* (1), 7−15.
(46) Yang, G.; Park, S.-J. Facile Hydrothermal Synthesis of NiCo2O4- Decorated Filter Carbon as Electrodes for High Performance Asymmetric Supercapacitors. *Electrochim. Acta* **2018**, *285*, 405−414.
(47) Senthil, R. A.; Jung, S.; Min, A.; Kumar, A.; Moon, C. J.; Singh, M.; Choi, M. Y. Revealing the Impact of Pulsed Laser-Produced Single-Pd Nanoparticles on a Bimetallic $NiCo_2O_4$ Electrocatalyst for Energy-Saving Hydrogen Production via Hybrid Water Electrolysis. *ACS Catal.* **2024**, *14* (5), 3320−3335.
(48) Waghmode, R. B.; Maile, N. C.; Lee, D. S.; Torane, A. P. Chemical Bath Synthesis of NiCo2O4 Nanoflowers with Nanorods like Thin Film for Flexible Supercapacitor Application-Effect of Urea Concentration on Structural Conversion. *Electrochim. Acta* **2020**, *350*, No. 136413.
(49) Liu, Z.-Q.; Xu, Q.-Z.; Wang, J.-Y.; Li, N.; Guo, S.-H.; Su, Y.-Z.; Wang, H.-J.; Zhang, J.-H.; Chen, S. Facile Hydrothermal Synthesis of Urchin-like NiCo2O4 Spheres as Efficient Electrocatalysts for Oxygen Reduction Reaction. *Int. J. Hydrogen Energy* **2013**, *38* (16), 6657−6662.
(50) Chang, C.; Zhang, L.; Hsu, C.-W.; Chuah, X.-F.; Lu, S.-Y. Mixed NiO/$NiCo_2O_4$ Nanocrystals Grown from the Skeleton of a 3D Porous Nickel Network as Efficient Electrocatalysts for Oxygen Evolution Reactions. *ACS Appl. Mater. Interfaces* **2018**, *10* (1), 417−426.
(51) Sha, L.; Ye, K.; Wang, G.; Shao, J.; Zhu, K.; Cheng, K.; Yan, J.; Wang, G.; Cao, D. Hierarchical NiCo2O4 Nanowire Array Supported on Ni Foam for Efficient Urea Electrooxidation in Alkaline Medium. *J. Power Sources* **2019**, *412*, 265−271.
(52) Zuo, Y.; Bellani, S.; Saleh, G.; Ferri, M.; Shinde, D. V.; Zappia, M. I.; Buha, J.; Brescia, R.; Prato, M.; Pascazio, R.; Annamalai, A.; de Souza, D. O.; De Trizio, L.; Infante, I.; Bonaccorso, F.; Manna, L. Ru−Cu Nanoheterostructures for Efficient Hydrogen Evolution Reaction in Alkaline Water Electrolyzers. *J. Am. Chem. Soc.* **2023**, *145* (39), 21419−21431.
(53) Mardle, P.; Chen, B.; Liu, H.; Xie, Z.; Qu, W.; Holdcroft, S. Effects of Aemion and Aemion+ Binders in Oxygen Evolution Reaction Catalyst Layers. *Electrochim. Acta* **2025**, *528*, No. 146273.
(54) Ahmed, K. W.; Habibpour, S.; Chen, Z.; Fowler, M. Investigation of NiCoOx Catalysts for Anion Exchange Membrane Water Electrolysis: Performance, Durability, and Efficiency Analysis. *J. Energy Storage* **2024**, *79*, No. 110149.

https://doi.org/10.1021/acsaem.5c01487
ACS Appl. Energy Mater. XXXX, XXX, XXX−XXX